Interactive Multi-Stiffness Mixed Reality Interface: Controlling and Visualizing Robot and Environment Stiffness

Díaz Rosales, A.; Rodriguez-Nogueira, Jose; Matheson, Eloise; Abbink, D.A.; Peternel, L.

Interactive Multi-Stiffness Mixed Reality Interface: Controlling and Visualizing Robot and Environment Stiffness

Alejandro Díaz Rosales[1,2], Jose Rodriguez-Nogueira[1,3], Eloise Matheson[1],
David A. Abbink[2], and Luka Peternel[2]

Abstract— Teleoperation is a crucial technology enabling human operators to control robots remotely to perform tasks in hazardous and difficult-to-access environments. Tasks in such environments often involve complex physical interactions with tools and objects of various softness. To this end, teleimpedance enables the operators to adjust the robot impedance in real-time to simplify such interactions. While the existing teleimpedance approaches provide several interfaces to command the robot impedance, there are no interfaces to visualize both the commanded impedance and that of the objects to be interacted with. This paper presents a novel interface to provide visual feedback on the impedance of remote robots and objects. To do so, we use virtual stiffness ellipsoids and different modes that display the individual impedance of the robot and objects as well as combined post-contact impedance. The key advantage of visual feedback on the impedance compared to force feedback is that the operator can see the interaction characteristics before the contact occurs. This enables the operator to act proactively before contact rather than just reactively after the contact. This paper also proposes a new intuitive way to command the robot impedance using mixed reality, interacting with these ellipsoids and modifying them as needed. To demonstrate the key functionalities of the developed interface, we performed proof-of-concept experiments on teleoperated tasks.

I. INTRODUCTION

A major challenge for robotic systems is the ability to act in unknown environments, especially when involving physical interactions with objects that may have different properties in terms of shape and hardness. For instance, robot-assisted handling at CERN involves interacting with objects of varying material stiffness. In some cases, the involved robot may also use a flexible tool, or be flexible itself. This can make modeling difficult and, as a result, increase control complexity for the operator. Therefore, the next generation of robots must be capable of adapting their physical interaction control to various tasks under changing conditions [1], [2]. Tasks can be categorized into three groups: structured, semi-structured, and unstructured based on their unpredictability and environment. As the uncertainty increases, the modeling of interactions between the robot and the environment becomes more complex.

Robots and tools with low or adjustable stiffness are often used to perform tasks in unstructured and unpredictable environments. A common control technique for this is impedance
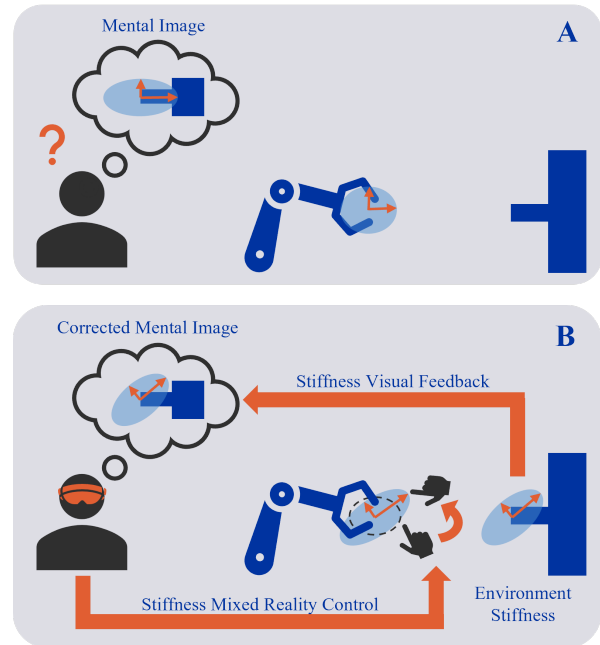

Fig. 1. Overview of the proposed Human-Robot Interface and its effects. In scenario A, the operator must rely on a mental image of the environment's stiffness, potentially leading to misconceptions and requiring guesswork for setting the robot impedance. On the other hand, scenario B features the proposed mixed reality interface that offers precise visual cues on stiffness while enabling intuitive impedance control. This interface facilitates direct interaction with the robot stiffness ellipsoid using hands, allowing adjustments tailored to the tasks and environments.

control [3], which was inspired by how humans adjust their limb impedance through muscle activity to perform various complex physical interaction tasks [4]. In the presence of unstable dynamic environments with perturbations or unwanted forces, humans learn how to make the interaction stable using an energy-efficient impedance control based on their muscle activation and limb configuration [5], [6].

In robotics, variable impedance control (VIC) enables simultaneous control of motions and contact forces through impedance regulation [7]. This advancement enhances overall task performance while ensuring the robot's and its surrounding's safety [8]. For example, in delicate and unstable environments the robot can become more compliant to mitigate high-impact forces effectively. Alternatively, when performing a task that requires accuracy, it is recommended to increase the impedance to reject any unpredictable perturbations [9], [10], [11].

The problem of operating in an unstructured and unpredictable environment is especially prominent in tasks such

[1]European Organization for Nuclear Research (CERN), Espl. des Particules 1, 1211 Meyrin, Switzerland.

[2]Department of Cognitive Robotics, Delft University of Technology, Mekelweg 2, 2628 CD Delft, The Netherlands.

[3]Centro de Automatica y Robotica (CAR) UPM-CSIC, Universidad Politecnica de Madrid, 28006 Madrid, Spain.

E-mail: alejandro.diaz.rosales@cern.ch

as remote robot maintenance, where the operator has to control a distant robot through an interface [12], [13], [14], [15]. To this end, teleimpedance is used to enable remote control of impedance in teleoperation [16]. For example, the interface to control the remote robot's impedance can be based on measuring the operator's muscle activity to map human impedance to the robot [17], [18], [19], [20]. Another example is to induce perturbations on the operator's arm by a haptic device and measure the corresponding motion to estimate the impedance [21]. Force grip can also be used as an estimate of overall arm impedance [8]. Alternatively, more practical interfaces such as buttons/sliders [22], [23] or tablets [24] can also be employed. If force feedback is employed, the operator can also feel the commanded impedance [22], [25], which can help with the execution of tasks. However, force feedback is not always available and the operator can only react to it after already touching the object. A visual way of presenting impedance could help the operator plan for the interaction before it occurs.

In the context of VIC, the element that is often changed is the stiffness. The most common way to graphically represent the endpoint stiffness of manipulators is by using ellipsoids. There is the isopotential ellipse [26] and the stiffness ellipse [27]. An alternative approach to represent stiffness is through Mohr's Circle, as shown by English and Russell [26]. This method provides more detailed information compared to ellipses and it can be used in cases where the manipulator stiffness is unstable or contains anti-symmetric components. However, despite its advantages, Mohr's Circles are not used in variable impedance control due to their complexity. The robot operator needs more time to understand the information it contains. In contrast to ellipses, Mohr's Circles cannot be plotted in the manipulator workspace.

Stiffness ellipsoids are often used to visualize the manipulator's impedance in an offline manner for a post-experiment analysis [27], [28], [6]. The method described in [24] designed an interface for teleimpedance that can provide visual feedback of the commanded impedance online in real-time. The interface included a tablet that displayed an image of two ellipses representing the stiffness ellipsoid. The operator could adjust the shape, size, and orientation of these ellipses to achieve the desired stiffness. This device could also be utilized to visualize the ellipsoid in tasks where stiffness is automatically adapted according to the task. However, the operator had to focus solely on the tablet to receive feedback, which meant they had to divert their attention away from the real robot or the remote camera feed that displayed the visual feedback of the task. Importantly, the interface displayed only the commanded robot impedance and not that of the objects the robot interacts with.

Improving the representation of stiffness can improve the user's control of stiffness for teleimpedance. The interface mentioned before [24] proved that modifying the ellipses is an innovative way to precisely control the stiffness in the three axes of the robot, with no coupling effect [29]. However, one main issue is that it takes time for users to understand the direction in which the impedance needs to be changed. This requires matching the ellipsoid reference frame with the robot's frame, which can be challenging. Furthermore, changing the orientation of the ellipse among multiple axes requires several steps, slowing down the operator. The other main issue is that this approach does not provide information about the stiffness of the environment.

To address these two gaps, this paper aims to investigate how we can enhance the user experience by developing a 3D interface able to represent both the robot and environment impedances through virtual stiffness ellipsoids. We explore ways to adapt this interface to diverse hardware configurations, ranging from traditional screens to augmented reality (AR) headsets. Particularly, in the latter setup, users have the capability to interact directly with these ellipsoids using their hands to control robot impedance (Fig. 1). The sections II, III and IV describe the design process and the functionalities of the interface. Finally, proof of concept experiments are presented in Sec. V.

II. BACKGROUND

In robot modeling and control, the impedance of a system can be represented using a mass-spring-damper model. This model is commonly used to describe the behavior of a mechanical system at a certain point, such as a robot end effector, when it interacts with its environment. The impedance control law is given as

$$\boldsymbol{F} = \boldsymbol{M}(\ddot{\boldsymbol{x}}_r - \ddot{\boldsymbol{x}}) + \boldsymbol{D}(\dot{\boldsymbol{x}}_r - \dot{\boldsymbol{x}}) + \boldsymbol{K}(\boldsymbol{x}_r - \boldsymbol{x}), \qquad (1)$$

where $\boldsymbol{F}$ is the interaction force acting from the robot on the environment. The vectors $\boldsymbol{x}_r$ and $\boldsymbol{x}$ describe the reference and the actual pose of the robot end effector and are local coordinates which is valid and singularity-free for small errors. The error is defined on the Lie group $SE(3)$, representing the pose using homogeneous transformation [30]. $\boldsymbol{M} \in \mathbb{R}^{6 \times 6}$, $\boldsymbol{D} \in \mathbb{R}^{6 \times 6}$ and $\boldsymbol{K} \in \mathbb{R}^{6 \times 6}$ are the inertia tensor, damping, and stiffness matrices, respectively. It is important to note that in the context of VIC, the element that is often changed is stiffness. Higher-order elements beyond inertia are not considered, as inertia itself is often excluded in practical implementations. Additionally, damping is commonly linked to the commanded stiffness to enhance system stability [31].

To provide input for the developed interface, there are different ways to estimate the stiffness of objects, such as tools and other items that a robot might interact with. This can be done before or during a task. In a known environment, the objects can be modeled and simulated to determine the right impedance parameters in advance. Alternatively, the robot's vision capabilities can be used to detect the environment characteristics [32]. Another option is to use haptic feedback where the system determines the object's impedance based on the forces that it encounters while interacting with it [10], [11]. However, the impedance can only be known after the physical interaction occurs.

We use ellipsoids to visually represent the stiffness, where the length from the center to the surface correlates to the stiffness value in that direction. This representation also makes it intuitive for humans to manipulate them [16].

III. Stiffness Visualization Interface

One objective of the developed interface is to exhibit the stiffness ellipsoids of both the robot and the environment using a 3D Human-Robot Interface as shown in scenario B of Fig. 1. The interface aims to display the ellipsoids directly on the points of interest, following their location and orientation. We used eigenvalues Σ and eigenvectors Q obtained from the eigendecomposition of the stiffness matrix as $K = Q\Sigma Q^T$ to derive size and orientation of the ellipsoids for the three axis directions. The developed interface does not use ellipsoids to display rotational stiffness.

We integrated six functionalities to provide visual feedback on the robot's interaction with the environment, each exhibiting stiffness ellipsoids in unique ways for different purposes, as explained in the following subsections.

A. Point Selection

A list of available points in space where the stiffness is known is shown to the user. The purpose of this initial step is to give the operator full control of what is going to be displayed during the task. Displaying all the available information can result in an extremely cluttered interface, negatively affecting the operator.

B. Compliance Representation

Instead of showing the stiffness ellipsoid, it is also possible to show the compliance ellipsoid of any desired point. This is simply done by inverting the stiffness matrix ($C = K^{-1}$) and doing the eigendecomposition to define the ellipsoid. It can be easier for users to understand compliance when objects in the environment have low stiffness. The interface shows the compliance ellipsoid in blue and the stiffness in orange.

C. Ellipsoid Scale

There are times when users may need to adjust the scale of an ellipsoid to improve its visibility. Some ellipsoids may be too small to see, while others might be too large. To guarantee improved visibility during operation, the ellipsoid can be increased or reduced by a factor of 10.

D. Enable/Disable Axes

One feature is the ability to turn off the representation of specific axes of an ellipsoid (Fig. 2). This is useful when the stiffness in any direction is not relevant or not important for the task and could overshadow the smaller stiffness values of other points. Users can then prioritize the most relevant information by choosing which information to display.

E. Change Ellipsoid Reference Frame

This feature enables the user to adjust the coordinate system used to represent the stiffness of a particular point. The original system, labeled as *A*, can be changed to a new reference frame, labeled as *B*. If we just consider the force applied by the stiffness we get:

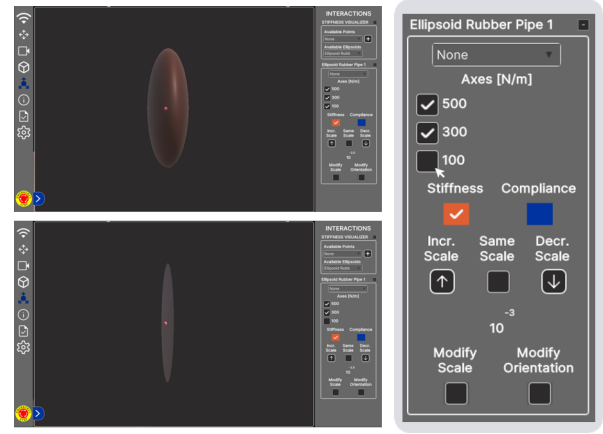$$^B\boldsymbol{F} = \,^B\boldsymbol{K}\left(^B\boldsymbol{x}_r - \,^B\boldsymbol{x}\right) \tag{2}$$

Fig. 2. Menu to enable or disable an axis in each available ellipsoid.

For nodal forces, the relation between them is:

$$^A\boldsymbol{F} = \,^A\boldsymbol{R}_B\,^B\boldsymbol{F} \tag{3}$$

Where $^A\boldsymbol{R}_B$ is the rotation matrix. Combining the two equations and knowing that R is orthogonal, meaning the inverse is equal to its transpose, we find:

$$^B\boldsymbol{K} = \,^A\boldsymbol{R}_B^T\,^A\boldsymbol{K}\,^A\boldsymbol{R}_B \tag{4}$$

A useful application of this option is to display the stiffness of the robot arm in the attached tool.

F. Ellipsoid Combination

In situations where the user chooses the same reference frame for two or more available points, the interface will consider that they have to be displayed together in the same ellipsoid (Fig. 3). To do this we will represent the resultant stiffness of all the springs connected in series by a rigid connection, as if they were in contact. If the two stiffness are represented in the same reference frame using equation 4, the principle of serials springs can be applied:

$$^B\boldsymbol{C}_{Combined} = \,^B\boldsymbol{C}_{P1} + \,^B\boldsymbol{C}_{P2} \tag{5}$$

In the form of stiffness:

$$^B\boldsymbol{K}_{Combined} = \left(^B\boldsymbol{K}_{P1}^{-1} + \,^B\boldsymbol{K}_{P2}^{-1}\right)^{-1} \tag{6}$$

The resulting ellipsoid illustrates the stiffness between two contact points, offering insight into the system behavior and allowing proactive measures by the user to avoid unexpected actions. A situation where this could be useful is when a robot ($\boldsymbol{K}_{P1}$) has a compliant tool ($\boldsymbol{K}_{P2}$) attached to it, and the operator wants to know the actual stiffness of the endpoint. The combined stiffness ($\boldsymbol{K}_{Combined}$) of the robot and the tool would give such information.

IV. Stiffness Commanded Interface

In a robotic setup prepared for teleimpedance control, once there is proper visualization of robot and environment stiffness ellipsoids, operators can effectively modify the VIC stiffness values to those that better suit the task (Scenario B of Fig. 1). Using mixed reality headsets, operators gain
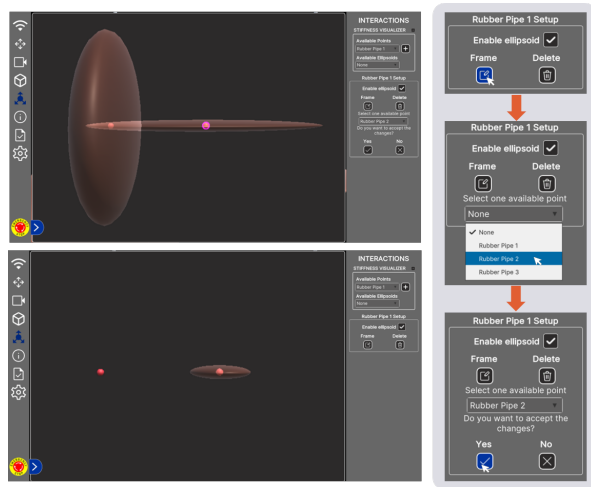
Fig. 3. Steps to follow in the interface to combine the ellipsoids in a single point by changing the reference frame.

Fig. 4. This is how the user sees the virtual stiffness ellipsoid with the AR headset and the two ways to modify it.

the ability to modify the virtual ellipsoids marked as controllable, such as the one of the robot (Fig. 4). The user can interact directly with the stiffness using the hands, intuitively adjusting the size and orientation. This approach allows operators to maintain focus on the task without taking their eyes off the robot.

The user can choose to resize or rotate the ellipsoid, but only one option can be selected at the same time to simplify interaction and minimize errors. If the user chooses to change the size, a reference frame appears with the value on each axis. The user can grab the arrow of the axis and move it to increase or decrease the corresponding value. The value of the axis changes as the user moves it. If the user selects the option to change the orientation, a box appears containing the ellipsoid. The user can grab points on this box to rotate the ellipsoid in any direction. Once the user is satisfied with the new ellipsoid, they can confirm the change by clicking on the "save" button. This sends the transformed ellipsoid back to the impedance controller and it can be done at any time during the task execution. The rotational stiffness cannot yet be controlled with this interactive method.

V. EXPERIMENTS

To demonstrate the capabilities of the interface we performed two proof-of-concept demonstration experiments. The purpose of the first experiment was to evaluate the visualization of stiffness, while the second aimed to evaluate the proposed interface for controlling stiffness ellipsoids. Both experiments were conducted by CERN's lead full-time robot teleoperator, who was given 30 minutes before each task to familiarize with the setup. After each experiment, the operator was asked to fill in the *Van der Laan* questionnaire [33] to evaluate the satisfaction and usefulness of the interface. We also conducted an interview where the operator could provide any additional feedback, impressions, and suggestions.

A Kinova Gen2 (6 DoF) was placed on a stable surface (Fig. 5). To provide visual feedback of the scene to the operator an Intel RealSense camera was mounted on the
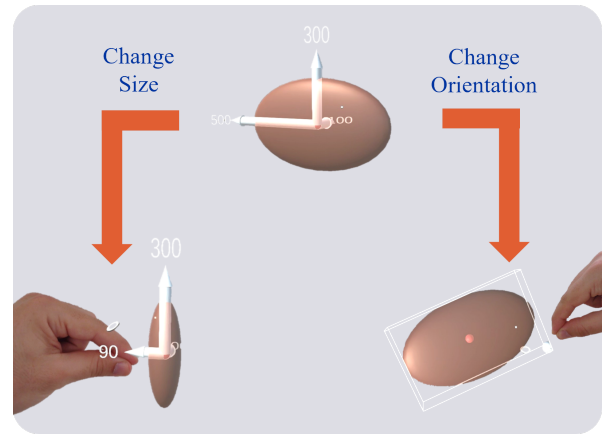
robot end effector. To measure the forces applied by the robot, a Medusa Force-Torque sensor from Bota Systems was also attached to the robot end effector. An environmental camera was also placed next to the base of the robot arm. All the devices were controlled using the CERN Robotic Framework (C++) [34] in a Linux system. In real CERN teleoperated maintenance activities, force feedback is not used yet due to potential instability problems that can affect task performance. These problems include low communication quality in certain areas and the impracticality of mobilizing the extra material required for force feedback. The operator often needs to move to specific areas where the communication between the robot and the operator's setup can be established, so installing extra components would increase the intervention time. For this reason, force feedback was also not employed in this experiment. The goal was to perform the test with a very minimal setup similar to those used in several tasks performed at CERN.

The 3D interface was developed with Unity, extending the capabilities of the existing CERN Robotic GUI [35], [36], [37]. While the interface can be used on a regular screen in its standard mode, we used the mixed reality modes displayed by Microsoft HoloLens 2 goggles to demonstrate all the functionalities of the interface. The human-robot user interface has two modes according to its hardware:

- *Basic Mode:* This is the simplest setup, in which the operator uses a screen to visualize the task information. A 3D representation of the robot is generated on the screen together with the ellipsoid. The current position of the robot and the values of the ellipsoid are updated in real- time. This mode can be used locally with the operator next to the robot or remotely.

- *Remote Mixed Reality Mode:* This mode takes the same 3D representation as in the previous mode but it uses AR headset to display it. This mode is thought to be used in cases where the operator can not see the real robot. The user wears the AR headset, which tracks the position of the operator's hands, so the performance of different tasks through gestures is possible. In this situation, the operator can move the 3D representation. This gives the
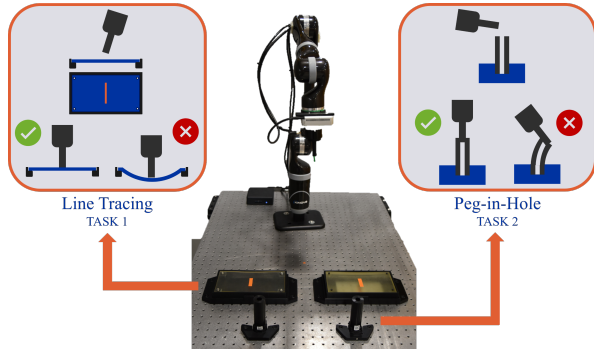
Fig. 5. Experiment setup with rubber plates and holes for the two tasks.

user more information about the position and orientation of the stiffness ellipsoid. A dynamic hologram menu appears when the user moves the hand up [36].

All the interface modes have the same visualization functionalities. The *Basic Mode* simply has it displayed on the screen, while the *Remote Mixed Reality Mode* can use a real or a virtual screen. For the control of the stiffness ellipsoids, only the *Remote Mixed Reality Mode* has the proposed functionality. For these demonstrations, we used the *Remote Mixed Reality Mode*.

The objects in Fig. 5 are explained in the following subsections in the experiments where they are used. During the experiments, the stiffness matrices are assumed to be diagonal for all available points in the visualizer.

A. Line Tracing: Environment Stiffness Visualization

The goal of this experiment was to test the effect of visualizing the environment's stiffness. The operator's task was to follow a line drawn on a flat surface as quickly as possible while maintaining contact and avoiding bending the surface. This task imitates various robotic activities such as cutting, polishing, drawing, or even more specific activities such as taking surface radiation samples with a piece of cotton, a common task at CERN.

The surface was made of a urethane plate (A50 shore hardness). There were two plates with a thickness of 6 mm and 20 mm, respectively. In the experiment, the plates were held by a support that prevented the user from knowing which plate was positioned where. The experiment aimed to compare the performance of the task with and without the ellipsoid visualization. To achieve this, the task was performed on both surfaces, one after the other, but the order was randomized (Fig. 6). The operator did the task three times for each visualization configuration. The plate's stiffness to be displayed in real-time by the visualizer was determined offline using the Ansys Simulation Software, assuming the center point of the plate as the point of contact. When the visualization was enabled, it was configured for the operator to see the compliance ellipsoids.

The results show that the interface provided clear advantages when the stiffness visualization was used, particularly when approaching the plates. Notably, the visualization helped to enter in contact with the 20 mm plate more quickly (approach time in Fig. 7), in contrast to the slower interaction
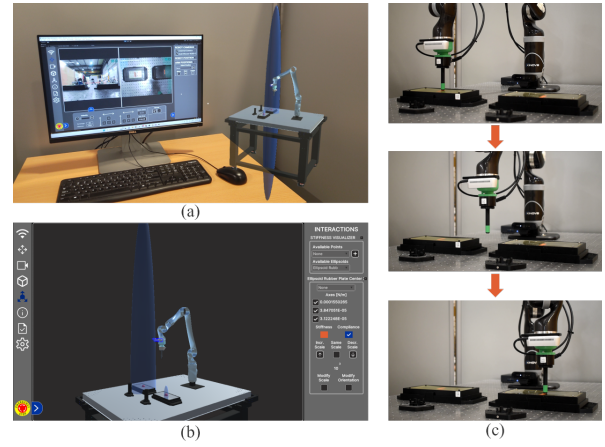

Fig. 6. Line tracing experiment. (a) Shows the operator view through the AR headset when the stiffness visualizer is enabled, showing the compliance ellipsoid of the two plates. (b) View of the interface in basic mode. (c) The procedure followed by the operator to execute the task.

observed with the 6 mm plate (approach time in Fig. 8). In post-experiment feedback, the operator explained that stiffness visualization enabled them to know which plate was which and use their experience to adapt the strategy for the specific plate. They could be faster and less careful when approaching the harder plate (20 mm), and slower when approaching the softer (6 mm) plate. However, when the visualization was disabled, the operator approached both plates with the same level of care, thus resulting in slower task execution for the harder plate (20 mm).

The tables I and II show an average of the results for each plate. The stiffness visualizer helped to reduce the average approach time to the 20 mm plate. Surprisingly, in the case of the 6 mm plate, it took more time with the visualizer. The operator performed the contact phase of the task faster with the visualizer for both plates. On average, it took the operator 135 seconds without the visualizer and 111 seconds with the visualizer to complete a full task using the two plates.

TABLE I

AVERAGE RESULTS WITH THE HARD PLATE (20 MM)

Condition	Disabled	Enabled
Approach Time [s]	74	25
Mean Force [N]	-8.3	-5.9
Deformation [mm]	4.5	2.5
Average Force Time [s]	19	12

TABLE II

AVERAGE RESULTS WITH THE SOFT PLATE (6 MM)

Condition	Disabled	Enabled
Approach Time [s]	25	44
Mean Force [N]	-0.7	-0.4
Deformation [mm]	3.4	3.5
Average Contact Time [s]	19	8

The results also indicate that using the stiffness visualizer causes a reduction of the forces applied to the plate surface. The operator commented that they had to rely on the camera feedback to determine whether contact had occurred or not. The contact was judged based on the visual deformation of the plate. The lack of information about the plate stiffness
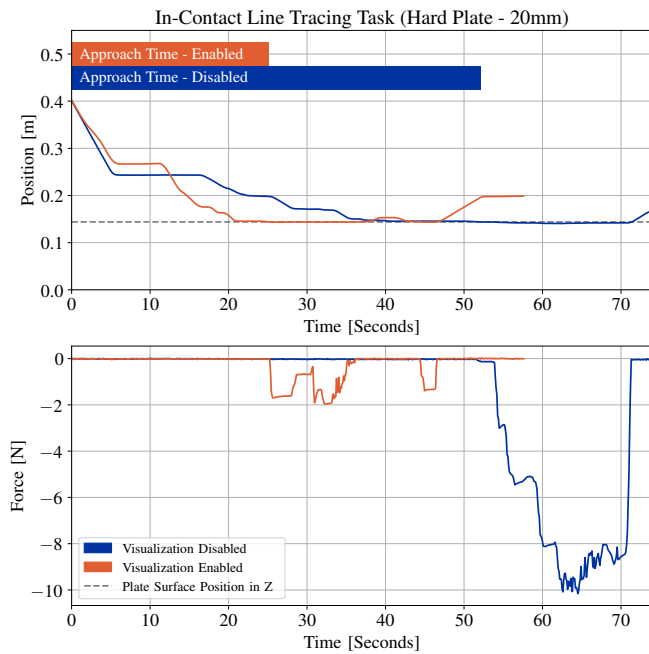
Fig. 7. Evolution of the position and force of the robot end effector in Z when executing the line tracing task with the plate of 20 mm. The horizontal bars show the time the operator took to approach the plate.
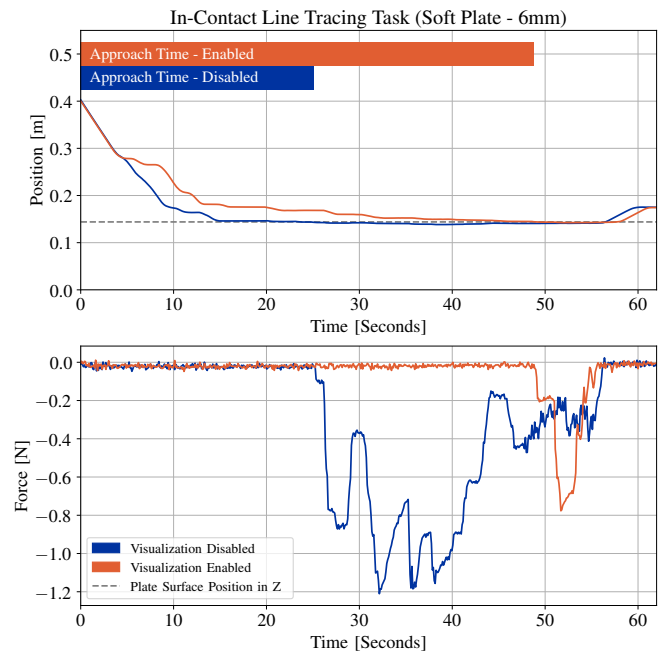

Fig. 8. Evolution of the position and force of the robot end effector in Z when executing the line tracing task with the plate of 6 mm. The horizontal bars show the time the operator took to approach the plate.

forced the operator to be more careful with how the bending was occurring. When the stiffness visualization was enabled, the operator was able to determine which material was harder and thus understood that waiting for visual deformation to confirm contact would create a larger force. Therefore, as soon as it looked like the robot was touching the hard plate (20 mm), they considered contact to have already occurred, resulting in a smaller force. This approach did not apply to the soft plate (6 mm) as the plate deformed more with a smaller contact force. This led the operator to use the bending of the plate as a visual clue to determine if there was contact.

To analyze the interface usefulness and satisfaction from the point of view of the main CERN robot operator, we used the *Van der Laan* questionnaire. The visualizer's improvement as rated by the operator is shown in Fig. 9.

B. Peg-in-Hole: Robot Stiffness Control

The goal of this experiment was to evaluate the effectiveness of the proposed interface for controlling stiffness ellipsoids. The operator had to perform a classic peg-in-hole task while avoiding any deformation of the objects (Fig. 10c). There were two holes made with a urethane tube, each with a different shore hardness A50 and A70. To increase the task difficulty, the operator did not have prior knowledge of the location of each visually indistinguishable tube. The operator had the ability to adjust the robot's stiffness while simultaneously observing the hole stiffnesses (Fig. 10a and 10b). This setup enabled a comprehensive evaluation of the interface's ability to facilitate precise and controlled interactions in dynamic environments.

Figure 11 shows how the stiffness ellipsoid changed in one of the attempts, as the operator was interacting with it. After the experiment, the operator filled again the *Van der Laan*
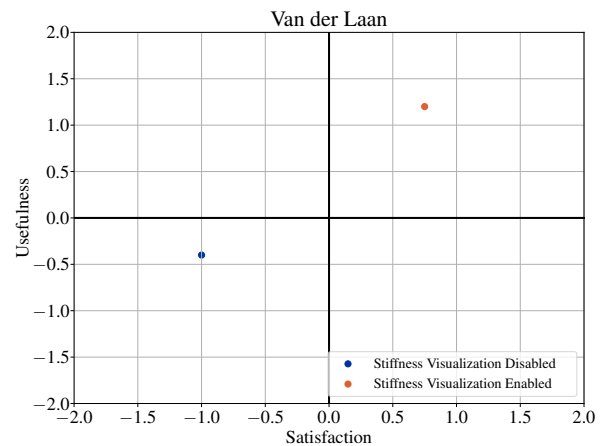

Fig. 9. The *Van der Laan* questionnaire has been used to compare operator perceived usefulness and satisfaction of the two interface configurations while performing the line tracing task. The blue dot represents the interface without stiffness visualization, while the orange dot represents the interface with stiffness visualization.

questionnaire resulting in a usefulness score of 1.2 and a satisfaction score of 0.5 (this result is not shown in a graph). The operator explained that the primary benefit of this control method is the intuitive visualization of the ellipsoid and how it aids the thinking process to determine the best stiffness for the task. It is also effortless to see the result of such changes. On the other hand, the operator suggested adding the possibility of giving the parameters using a keyboard for greater precision and voice commands for speed.

VI. DISCUSSION

We created a new teleimpedance interface that provides visual feedback about the robot and object impedance in a
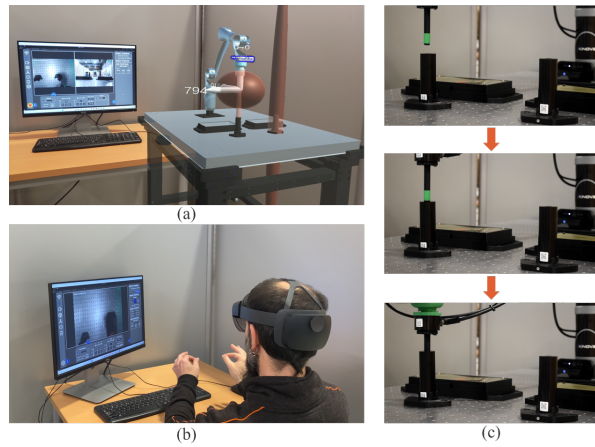
Fig. 10. Peg-in-Hole experiment. (a) Shows what the operator is seeing through the AR headset with the stiffness visualizer, showing the stiffness ellipsoid of the two holes and the one of the robot being modified. (b) The operator changes the size of the ellipsoid with the hands. (c) The procedure followed by the operator to execute the task in one of the holes.

remote environment and allows for more intuitive adjustment of the robot's impedance. This is the first interface that exploits mixed reality to visualize environment stiffness and to control the robot stiffness ellipsoid in teleimpedance. The visualization interface allows users to choose between a screen or an AR headset. The screen is simpler to set up, while the headset offers better understanding and immersion.

Visual feedback about the characteristics of physical interactions can serve as a complement to force feedback. While force feedback provides excellent information for the operator to act reactively based on the perceived forces at the haptic interface, the information is only available after the contact is already established. This makes it difficult for the operator to plan for the physical interaction of the remote robot with objects. Visual feedback has a key advantage over force feedback because it allows the operator to see the interaction characteristics before contact happens. This means the operator can take proactive action before the contact, rather than reacting after the contact.

Nevertheless, some things can be improved in the current solution. When there are many points too close to each other, it can be distracting and may obscure relevant elements necessary for the task. Even if the ellipsoids are stacked on top of each other, scaling down the size can only improve the situation to a certain extent. There comes a moment when valuable information about the ellipsoid may start to get lost. The user must decide if the ellipsoids have the same scale or not, requiring extra attention to avoid confusion. There is another problem that arises when the stiffness ellipsoid is significantly smaller on one axis compared to the others. If the smaller axis is the important one, then disabling the other axes will result in an extremely thin ellipsoid that can be difficult to visualize even when scaled up. For these types of objects, a better solution could be a heatmap that shows the stiffness at each point on the surface.

In this study, we employed an offline simulation-based method to estimate the impedance of the environment that
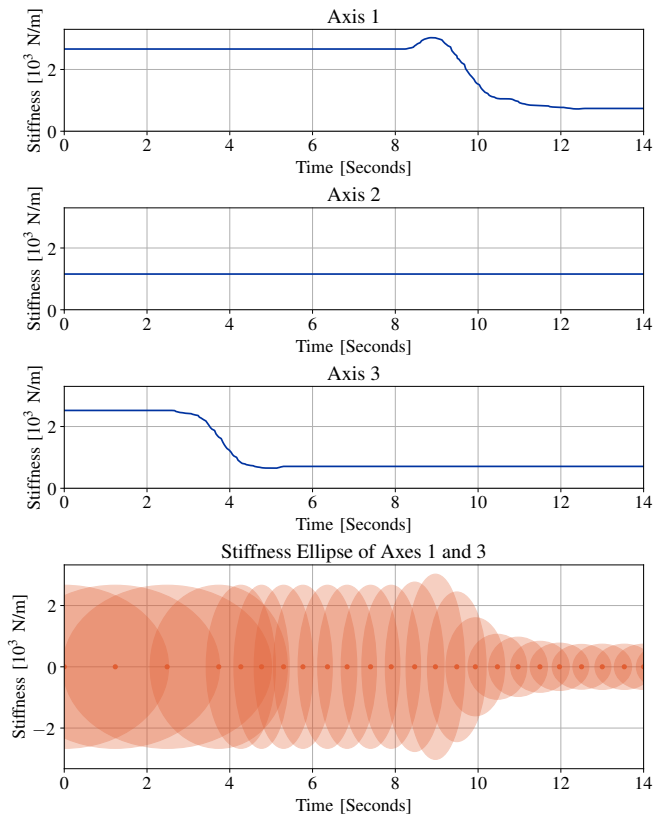

Fig. 11. Evolution of the robot stiffness when the operator decides to modify it. In this case, axis 2 corresponds to the direction of insertion of the hole, the operator makes the other two axes smaller to be more compliant so the robot adapts its position according to the hole. The last plot shows the evolution of the stiffness ellipse in those two axes.

is then displayed in real-time by the proposed interface. In future research, we will explore incorporating online vision-based methods for the estimation of impedance based on the object properties [32]. Such an addition would make the approach more robust for real-time changes in the environment.

The aim of this preliminary study was to develop the interface and demonstrate its main functionalities with proof-of-concept experiments. The experiments showed that the proposed solution for visualizing and adjusting the impedance using mixed reality functions as intended. The evaluation with an expert operator revealed that the interface is intuitive and that visualizing stiffness improves task safety and performance. The preliminary results indicate that interaction forces and execution times can be reduced by using information about stiffness. Nevertheless, the slight reduction in the approach time for the softer plate with the interface disabled was unexpected. This result might be due to the participation of only one individual and a limited number of trials.

For a better evaluation of the performance and usability of the developed interface, in the future, we will conduct an extensive human user study with multiple participants. We will also compare the operator performance between visualized stiffness feedback and force feedback. Furthermore, we will compare the proposed novel mixed reality interface for commanding stiffness ellipsoid to existing stiffness command interfaces from the state-of-the-art.

REFERENCES

[1] F. J. Abu-Dakka and M. Saveriano, "Variable impedance control and learning–a review," *Frontiers in Robotics and AI*, vol. 7, p. 590681, 2020.

[2] M. Suomalainen, Y. Karayiannidis, and V. Kyrki, "A survey of robot manipulation in contact," *Robotics and Autonomous Systems*, vol. 156, p. 104224, 2022.

[3] N. Hogan, "Impedance control: An approach to manipulation," *Journal of dynamic systems, measurement, and control*, vol. 107, no. 1, pp. 1–24, 1985.

[4] N. Hogan., "Adaptive control of mechanical impedance by coactivation of antagonist muscles," *IEEE Transactions on Automatic Control*, vol. 29, no. 8, pp. 681–690, Aug. 1984.

[5] E. Burdet, R. Osu, D. W. Franklin, T. E. Milner, and M. Kawato, "The central nervous system stabilizes unstable dynamics by learning optimal impedance," *Nature*, vol. 414, no. 6862, pp. 446–449, 2001.

[6] A. Naceri, T. Schumacher, Q. Li, S. Calinon, and H. Ritter, "Learning optimal impedance control during complex 3d arm movements," *IEEE Robotics and Automation Letters*, vol. 6, no. 2, pp. 1248–1255, 2021.

[7] P. Song, Y. Yu, and X. Zhang, "A Tutorial Survey and Comparison of Impedance Control on Robotic Manipulation," *Robotica*, vol. 37, no. 5, pp. 801–836, May 2019, publisher: Cambridge University Press.

[8] D. S. Walker, R. P. Wilson, and G. Niemeyer, "User-controlled variable impedance teleoperation," in *2010 IEEE International Conference on Robotics and Automation*, May 2010, pp. 5352–5357.

[9] S. Calinon, I. Sardellitti, and D. G. Caldwell, "Learning-based control strategy for safe human-robot interaction exploiting task and robot redundancies," in *2010 IEEE/RSJ International Conference on Intelligent Robots and Systems*, Oct. 2010, pp. 249–254.

[10] C. Yang, G. Ganesh, S. Haddadin, S. Parusel, A. Albu-Schaeffer, and E. Burdet, "Human-Like Adaptation of Force and Impedance in Stable and Unstable Interactions," *IEEE Transactions on Robotics*, vol. 27, no. 5, pp. 918–930, Oct. 2011.

[11] Y. Michel, R. Rahal, C. Pacchierotti, P. R. Giordano, and D. Lee, "Bilateral teleoperation with adaptive impedance control for contact tasks," *IEEE Robotics and Automation Letters*, vol. 6, no. 3, pp. 5429–5436, 2021.

[12] T. Sakaue, S. Yoshino, K. Nishizawa, and K. Takeda, "Survey in fukushima daiichi nps by combination of human and remotely-controlled robot," in *2017 IEEE International Symposium on Safety, Security and Rescue Robotics (SSRR)*, 2017, pp. 7–12.

[13] M. Bajracharya, M. W. Maimone, and D. Helmick, "Autonomy for mars rovers: Past, present, and future," *Computer*, vol. 41, no. 12, pp. 44–50, 2008.

[14] M. Di Castro, G. Lunghi, A. Masi, M. Ferre, and R. M. Prades, "A multidimensional rssi based framework for autonomous relay robots in harsh environments," in *2019 Third IEEE International Conference on Robotic Computing (IRC)*, 2019, pp. 183–188.

[15] M. Panzirsch, H. Singh, T. Krüger, C. Ott, and A. Albu-Schäffer, "Safe interactions and kinesthetic feedback in high performance earth-to-moon teleoperation," in *IEEE Aerospace Conference*, 2020, pp. 1–10.

[16] L. Peternel and A. Ajoudani, "After a Decade of Teleimpedance: A Survey," *IEEE Transactions on Human-Machine Systems*, vol. 53, no. 2, pp. 401–416, Apr. 2023.

[17] A. Ajoudani, M. Gabiccini, N. Tsagarakis, A. Albu-Schäffer, and A. Bicchi, "TeleImpedance: Exploring the role of common-mode and configuration-dependant stiffness," in *2012 12th IEEE-RAS International Conference on Humanoid Robots (Humanoids 2012)*, Nov. 2012, pp. 363–369.

[18] C. Yang, C. Zeng, P. Liang, Z. Li, R. Li, and C.-Y. Su, "Interface design of a physical human-robot interaction system for human impedance adaptive skill transfer," *IEEE Transactions on Automation Science and Engineering*, vol. 15, no. 1, pp. 329–340, 2017.

[19] S. Park, W. Lee, W. K. Chung, and K. Kim, "Programming by demonstration using the teleimpedance control scheme: Verification by an semg-controlled ball-trapping robot," *IEEE Transactions on Industrial Informatics*, vol. 15, no. 2, pp. 998–1006, 2018.

[20] S. Buscaglione, N. L. Tagliamonte, G. Ticchiarelli, G. Di Pino, D. Formica, and A. Noccaro, "Tele-impedance control approach using wearable sensors," in *2022 44th Annual International Conference of the IEEE Engineering in Medicine & Biology Society (EMBC)*. IEEE, 2022, pp. 2870–2873.

[21] G. Gourmelen, B. Navarro, A. Cherubini, and G. Ganesh, "Human guided trajectory and impedance adaptation for tele-operated physical assistance," in *2021 IEEE/RSJ International Conference on Intelligent Robots and Systems (IROS)*, 2021, pp. 9276–9282.

[22] L. Peternel, T. Petrič, and J. Babič, "Robotic assembly solution by human-in-the-loop teaching method based on real-time stiffness modulation," *Autonomous Robots*, vol. 42, no. 1, pp. 1–17, Jan. 2018.

[23] V. R. Garate, S. Gholami, and A. Ajoudani, "A scalable framework for multi-robot tele-impedance control," *IEEE Transactions on Robotics*, vol. 37, no. 6, pp. 2052–2066, 2021.

[24] L. Peternel, N. Beckers, and D. A. Abbink, "Independently Commanding Size, Shape and Orientation of Robot Endpoint Stiffness in Tele-Impedance by Virtual Ellipsoid Interface," in *2021 20th International Conference on Advanced Robotics (ICAR)*, Dec. 2021, pp. 99–106.

[25] M. Laghi, A. Ajoudani, M. G. Catalano, and A. Bicchi, "Unifying bilateral teleoperation and tele-impedance for enhanced user experience," *The International Journal of Robotics Research*, vol. 39, no. 4, pp. 514–539, Mar. 2020.

[26] C. E. English and D. L. Russell, "Representations of multi-joint stiffness for prosthetic limb design," *Mechanism and Machine Theory*, vol. 43, no. 3, pp. 297–309, Mar. 2008.

[27] F. Mussa-Ivaldi, N. Hogan, and E. Bizzi, "Neural, mechanical, and geometric factors subserving arm posture in humans," *The Journal of Neuroscience*, vol. 5, no. 10, pp. 2732–2743, Oct. 1985.

[28] E. Burdet, R. Osu, D. W. Franklin, T. E. Milner, and M. Kawato, "The central nervous system stabilizes unstable dynamics by learning optimal impedance," *Nature*, vol. 414, no. 6862, pp. 446–449, Nov. 2001.

[29] L. M. Doornebosch, D. A. Abbink, and L. Peternel, "Analysis of Coupling Effect in Human-Commanded Stiffness During Bilateral Tele-Impedance," *IEEE Transactions on Robotics*, vol. 37, no. 4, pp. 1282–1297, Aug. 2021.

[30] H. Gamper, L. Rodrigo Pérez, A. Mueller, A. Díaz Rosales, and M. Di Castro, "An inverse kinematics algorithm with smooth task switching for redundant robots," *IEEE Robotics and Automation Letters*, vol. 9, no. 5, pp. 4527–4534, 2024.

[31] A. Albu-Schaffer, C. Ott, U. Frese, and G. Hirzinger, "Cartesian impedance control of redundant robots: Recent results with the dlr-light-weight-arms," in *2003 IEEE International conference on robotics and automation*, vol. 3, 2003, pp. 3704–3709.

[32] Y.-C. Huang, D. A. Abbink, and L. Peternel, "A Semi-Autonomous Tele-Impedance Method based on Vision and Voice Interfaces," in *2021 20th International Conference on Advanced Robotics (ICAR)*, Dec. 2021, pp. 180–186.

[33] J. D. Van Der Laan, A. Heino, and D. De Waard, "A simple procedure for the assessment of acceptance of advanced transport telematics," *Transportation Research Part C: Emerging Technologies*, vol. 5, no. 1, pp. 1–10, 1997.

[34] M. Di Castro, M. Ferre, and A. Masi, "Cerntauro: A modular architecture for robotic inspection and telemanipulation in harsh and semi-structured environments," *IEEE Access*, vol. 6, pp. 37 506–37 522, 2018.

[35] G. Lunghi, R. M. Prades, and M. D. Castro, "An advanced, adaptive and multimodal graphical user interface for human-robot teleoperation in radioactive scenarios," in *ICINCO*. Setubal, PRT: SCITEPRESS - Science and Technology Publications, Lda, 2016, p. 224–231.

[36] K. A. Szczurek, R. M. Prades, E. Matheson, J. Rodriguez-Nogueira, and M. D. Castro, "Multimodal multi-user mixed reality human–robot interface for remote operations in hazardous environments," *IEEE Access*, vol. 11, pp. 17 305–17 333, 2023.

[37] K. A. Szczurek, R. M. Prades, E. Matheson, J. Rodriguez-Nogueira, and M. Di Castro, "Mixed reality human–robot interface with adaptive communications congestion control for the teleoperation of mobile redundant manipulators in hazardous environments," *IEEE Access*, vol. 10, pp. 87 182–87 216, 2022.